ANL/ET/CP--87316
CONF-9510156--11

Environmentally Assisted Cracking of LWR Materials*

O. K. Chopra, H. M. Chung, T. F. Kassner, and W. J. Shack

Argonne National Laboratory
Argonne, Illinois 60439

December 1995

DISCLAIMER

Proceedings of 23rd Water Reactor Safety Information Meeting, October 23–25, 1995, Bethesda, MD

*Work sponsored by the U. S. Nuclear Regulatory Commission, Office of Nuclear Regulatory Research, under Interagency Agreement DOE 40-550-75.

* Job Code A2212; NRC Program Manager: Dr. M. McNeil

Environmentally Assisted Cracking of LWR Materials*

O. K. Chopra, H. M. Chung, T. F. Kassner, and W. J. Shack
Argonne National Laboratory
Argonne, Illinois

Abstract

Research on environmentally assisted cracking (EAC) of light water reactor materials has focused on (a) fatigue initiation in pressure vessel and piping steels, (b) crack growth in cast duplex and austenitic stainless steels (SSs), (c) irradiation–assisted stress corrosion cracking (IASCC) of austenitic SSs, and (d) EAC in high–nickel alloys. The effect of strain rate during different portions of the loading cycle on fatigue life of carbon and low-alloy steels in 289°C water was determined. Crack growth studies on wrought and cast SSs have been completed. The effect of dissolved-oxygen concentration in high-purity water on IASCC of irradiated Type 304 SS was investigated and trace elements in the steel that increase susceptibility to intergranular cracking were identified. Preliminary results were obtained on crack growth rates of high–nickel alloys in water that contains a wide range of dissolved oxygen and hydrogen concentrations at 289 and 320°C.

The program on Environmentally Assisted Cracking of Light Water Reactor Materials is currently focused on four tasks: fatigue initiation in pressure vessel and piping steels, fatigue and environmentally assisted crack growth in cast duplex and austenitic SS, irradiation–assisted stress corrosion cracking of austenitic SSs, and environmentally assisted crack growth in high–nickel alloys. Measurements of corrosion–fatigue crack growth rates (CGRs) of wrought and cast stainless steels has been essentially completed. Recent progress in these areas is outlined in the following sections.

Irradiation Assisted Stress Corrosion Cracking

Failures of reactor–core internal components in both BWRs and PWRs have occurred after accumulation of relatively high fluence (>5 x 10^{20} n·cm^{-2}, E >1 MeV). As neutron fluence increases, initially nonsensitized austenitic SSs can become susceptible to intergranular failure. This type of degradation is commonly referred to as irradiation–assisted stress corrosion cracking (IASCC). Although most failed components can be replaced, some components would be very difficult or impractical to replace.

Heat-to-heat variations in susceptibility to IASCC have been observed to be very significant, even among high–purity (HP) materials containing virtually identical chemical compositions. Although radiation–induced grain-boundary Cr depletion is believed by most investigators to play an important role in IASCC, additional deleterious processes may be associated with trace impurities that are not usually identified in material specifications. Such trace elements could be introduced during steelmaking processes or during fabrication and welding.

* Job Code A2212; NRC Program Manager: Dr. M. McNeil

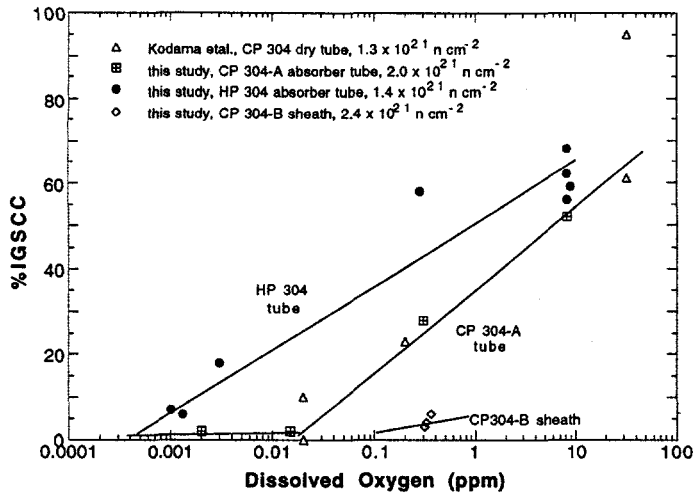

Figure 1.
Percent IGSCC vs. DO for HP and CP Type 304 SS neutron–absorber tubes (this study) and CP Type 304 SS dry tubes (Kodama et al.). Three distinct trends in DO dependence are evident.

Slow–strain–rate–tensile (SSRT) tests in simulated BWR environments on high- and commercial-purity (HP and CP) Type 304 SS were performed to determine the effects of water chemistry on susceptibility to IASCC. To obtain some insight into the mechanism(s) of IASCC, we attempted to correlate the susceptibility to intergranular cracking determined by SSRT tests with results of microchemical analysis of grain boundaries by Auger electron spectroscopy (AES).

The effect of dissolved oxygen (DO) in HP water on the susceptibility of irradiated materials to IASCC is shown in Fig. 1 for HP and CP neutron–absorber tubes and a control–blade sheath (fabricated from another CP–grade heat). Negligible IGSCC was observed in specimens from the control–blade sheath for all fluence levels; therefore, no tests were conducted to investigate the effect of DO, other than at ≈0.3 ppm. Results obtained by Kodama et al.,[1,2] are also shown for comparison. The effect of electrochemical potential (ECP) on the susceptibility of irradiated materials to IASCC is shown in Fig. 2 along with some results by Indig et al.[3] The effect of DO level and ECP on IASCC appears to be different for the HP and CP materials. The HP heats were less sensitive to DO level and ECP and were more susceptible to IASCC than the CP heats for all DO and fluence levels. No IASCC was observed in the CP heats for ECP <–140 mV SHE and DO <0.01 ppm.

The HP absorber specimen that exhibited a surprisingly high susceptibility to IGSCC of ≈18% at a very low DO of ≈0.002 ppm (Fig. 1) and ECP of ≈–320 mV SHE (Fig. 2) was examined in detail by AES. An intergranular (IG) region on the fracture surface was sputtered to a depth of ≈60 nm, and AES spectra were obtained as a function of depth from the fracture surface. Unexpected concentrations of F, Ca, B, Zn, and Al were observed in the AES spectra. Al was used as a deoxidizer during melting of the HP–grade SS and Ca could have originated from CaF_2 that may have been used as flux in melting HP SS. The B and Zn on the fracture surface was probably picked up from the water.

As shown in Fig. 3, a higher level of fluorine on grain boundaries may be associated with higher susceptibility to IASCC.[4] Inadvertent contamination of reactor components by fluorine could occur during pickling (in a solution containing HF) in the case of tubular components such as neutron–absorber–rod tubes, and by an F–containing weld flux in the case of large welded components such as BWR core shrouds and certain older top guides. A synergistic effect of a lower concentration of Cr and a higher concentration of fluorine on grain boundaries on susceptibility to IGSCC is consistent with IGSCC results by Ward et al.[5]

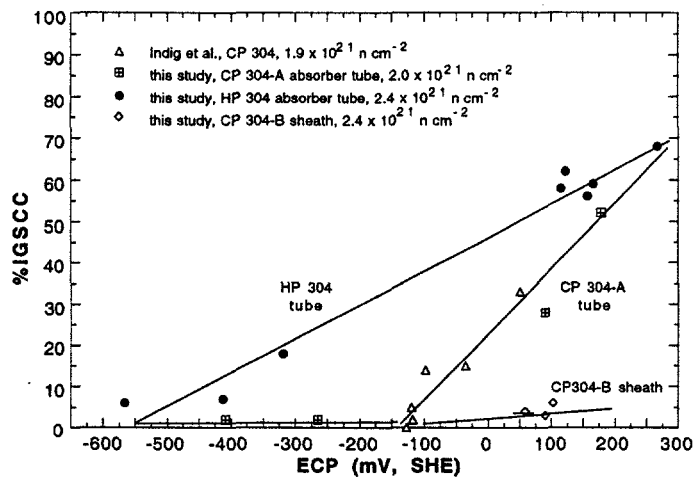

Figure 2.
Percent IGSCC vs. ECP of HP and CP Type 304 SS neutron–absorber tubes (this study) and CP Type 304 SS BWR sheet material (Indig et al.)

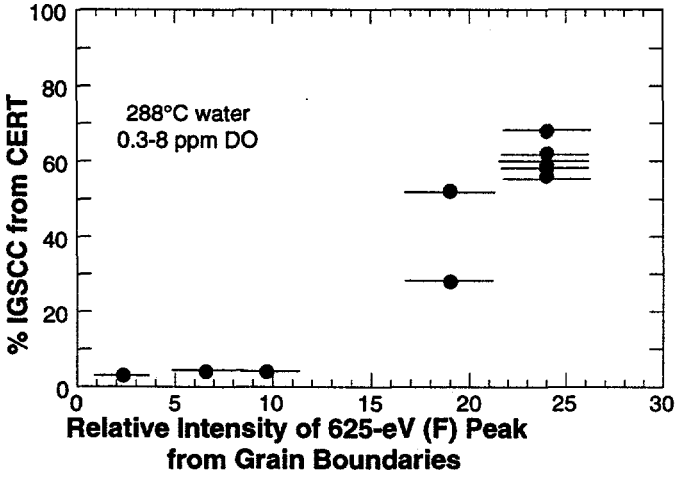

Figure 3.
Percent IGSCC vs. average intensity of fluorine signal from grain boundaries of HP and CP Type 304 SS BWR components

They reported fluorine–accelerated IGSCC of nonirradiated thermally sensitized bend specimens and weldments of CP–grade Type 304 SS that were contaminated with a fluorine–containing weld flux. They also reported that fluorine–assisted IGSCC was less sensitive to DO compared to classical IGSCC of thermally sensitized fluorine–free specimens, which is consistent with our present results.

Halide impurities play a catalytic role in accelerating aqueous corrosion of Fe and Fe–base alloys but their influence can be strongly mitigated by the concentration of Cr ions in water.[6] The corrosion acceleration has been attributed to the rate of formation of ligand complex between Fe–halide (i.e., halide anion chemisorbed on Fe) and H_2O molecules, which has rate several orders of magnitude higher than the rate of formation of a similar ligand complex between halide–free Fe atoms and H_2O molecules.[6] A similar effect can be postulated for relative reaction rates to form fluorine–containing and fluorine–free ligand complexes of $FeF(H_2O)_5$ and $Fe(H_2O)_5$, respectively. A halide atom is released from the labile ligand complex [e.g., $FeF(H_2O)_5$] dissolved in water when H_2O replaces the halide atom in the complex, thus leading to a classical catalysis by halides. However, this reaction chain is broken when the concentration of Cr ions in water is high (e.g., at a crack tip in which grain boundaries exhibit minimal Cr depletion), because Cr–halide–H_2O ligand complex [e.g., $CrF(H_2O)_5$] forms rapidly but remains inert in water. This inhibits a catalytic role of the halide atoms (e.g., fluorine atoms). According to this model, several key

factors that could influence susceptibility to IASCC are: the concentration of free halide atoms (e.g., fluorine) available on grain boundaries (i.e., those not trapped by stable precipitates[7] or compounds), the concentration of Cr ions in water at the crack tip, and the lability of $FeF_x(H_2O)_y$ complex under irradiation in LWR water.

The above hypotheses seems to be consistent not only with the behavior of HP–grade neutron–absorber tubes (high susceptibility) and CP–grade control–blade sheath (negligible susceptibility) observed in our study but also with increased susceptibility to IGSCC of fluorine–contaminated welds of either nonirradiated or irradiated Type 304 SS. However, it is too early to make a conclusive statement regarding its validity and applicability to cracking of LWR core–internal components. Nonetheless, irradiation–induced grain–boundary depletion of Cr and contamination and segregation of halides (most likely fluorine) during component fabrication appear to be the two key processes that may produce synergistic effects leading to increased susceptibility to IASCC. Compared to nonirradiated and solution–annealed material, the synergistic effect will be undoubtedly more pronounced for materials in which yielding in the grain matrix is relatively more difficult as a result of hardening by either irradiation or cold work.

Fatigue of LWR Structural Materials

The ASME Boiler and Pressure Vessel Code provides rules for the construction of nuclear power plant components. Appendix I to Section III of the Code specifies fatigue design curves for structural materials. The effects of reactor coolant environments are not explicitly addressed by these design curves, although test data illustrate potentially significant effects of LWR environments on the fatigue resistance of carbon and low–alloy steels.

Interim fatigue design curves that account for environmental effects were presented in NUREG/CR–5999. A more rigorous statistical analysis of the available data was developed in NUREG/CR–6335. One important conclusion derived from our test program and a rigorous review of the available data is that a minimum strain appears to be required for environmentally assisted decrease in fatigue life. This threshold strain may vary with material and loading conditions such as steel type, temperature, DO, strain ratio, mean stress, etc., but for both A106–Gr B carbon steel and A533–Gr B low–alloy steel used in our present study, the threshold strain range is ≈0.36%.

Although the correlations in NUREG/CR–5999 and NUREG/CR–6335 are in excellent agreement with available laboratory data for loading histories with constant strain amplitudes and constant strain rates during the tensile portion of the loading cycle, actual loading histories are far more complex. Exploratory fatigue tests are being conducted with waveforms where the slow strain rate is applied during only a fraction of the tensile loading cycle. The results of such tests will be used to develop a "damage rule" that can be used to predict life under complex loading histories.

The results of tests on A106–Gr B steel at ≈0.75% strain range under a variety of loading waveforms are summarized in Fig. 4. The histories consist of segments of loading and unloading at fast and slow strain rates. The variation in fatigue life of A106–Gr B and A533–Gr B steels as a function of the fraction of loading strain at slow strain rate is shown in Fig. 5; results from tests conducted at Ishikawajima–Harima Heavy Industries Co. (IHI) on the ANL heat of A106–Gr B steel are also included in the figure. Open symbols indicate tests where the slow portions occurred near the maximum tensile strain. Closed symbols indicate tests where the slow portions occurred near the maximum compressive strain. In stroke–controlled

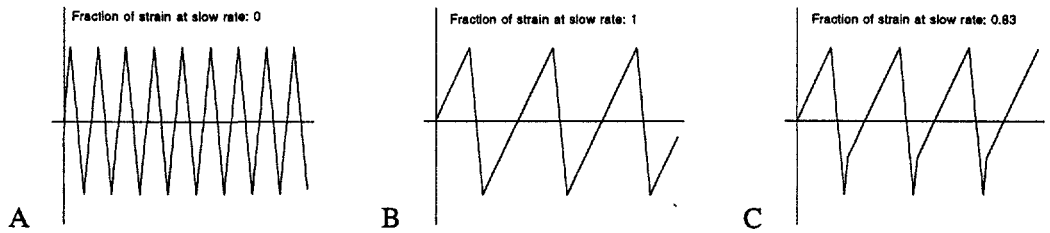

A

Air: 3,253; 3,753
PWR: 2,230; 1,525
Hi DO: 2,077; 1,756

B

Air: 3,721; 3,424; 6,275
PWR: 2,141
Hi DO: 303; 469

C

Air: 3,893
PWR: –
Hi DO: 340

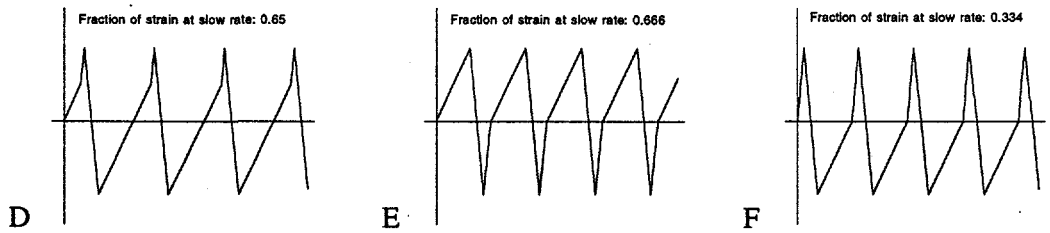

D

Air: 4,356
PWR: –
Hi DO: 615

E

Air: 5,261

F

Air: –
PWR: –
Hi DO: 1,935

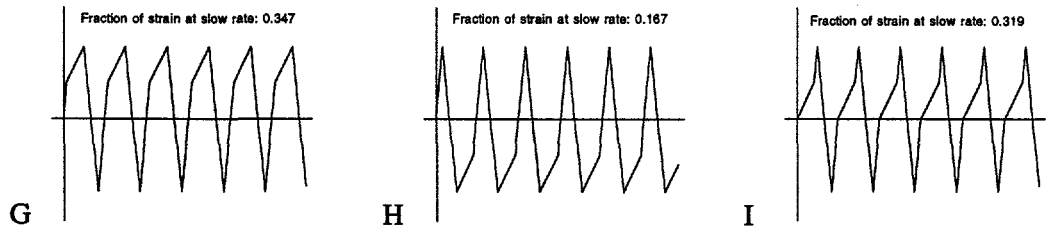

G

Air: 5,139
PWR: –
Hi DO: 615; 553

H

Air: 4,087
PWR: –
Hi DO: 1,649; 2,080

I

Air: 5,240
PWR: –
Hi DO: 1,306

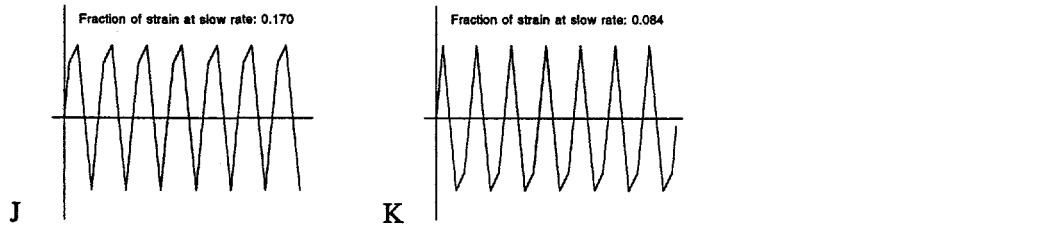

J

Air: 4,122
PWR: –
Hi DO: 888

K

Air: 4,105
PWR: –
Hi DO: 2,093

Figure 4. Fatigue life of A106–Gr B carbon steel at 288°C and 0.75% strain range in air and water under different loading waveforms

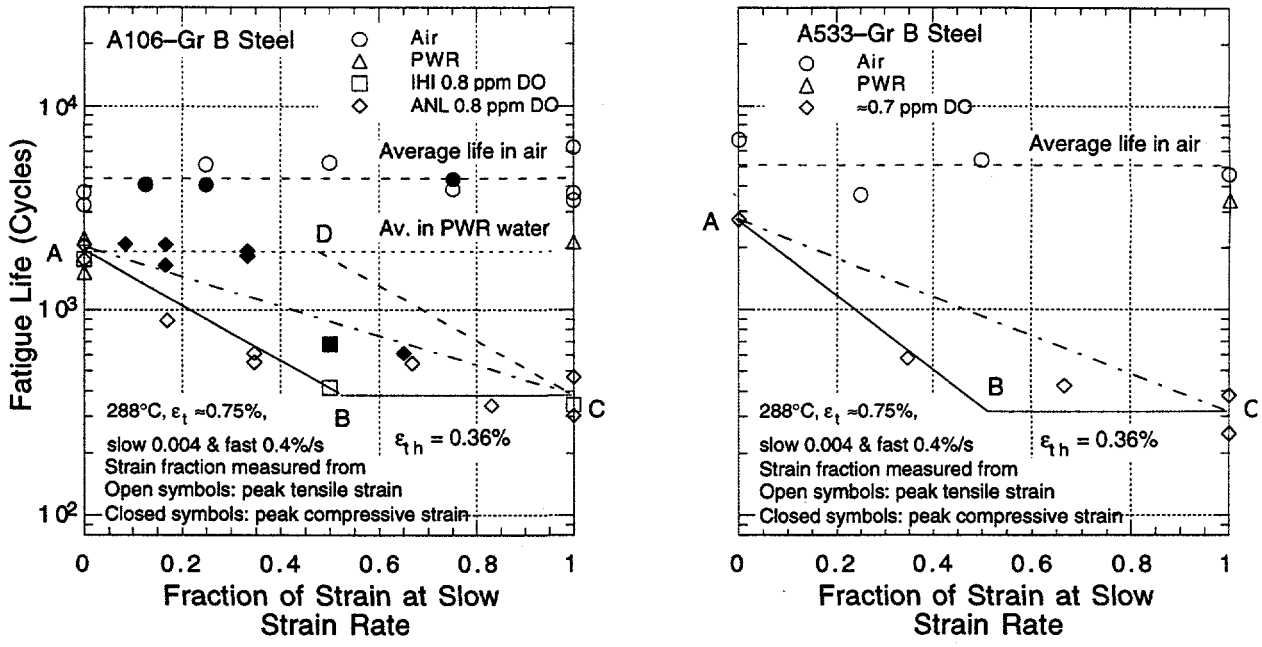

Figure 5. Fatigue life of A106–Gr B and A533–Gr B steels tested with loading waveforms where slow strain rate is applied during a fraction of tensile loading cycle

tests, the fraction of loading strain that is actually applied to the specimen gage section is not constant but varies during the cycle. For example, for waveforms E and F, although 0.5 of the applied displacement is at a slow rate, the actual fractions of strain at slow rate in the specimen gage section are 0.666 and 0.334, respectively.

The results to date suggest that a slow strain rate applied during any portion of the loading cycle above the threshold strain is equally effective in decreasing fatigue life, i.e., the relative damage due to the slow strain rate is independent of the strain amplitude once the amplitude exceeds the threshold value.[8–10] This can be demonstrated using the results shown in Fig. 5. If the relative damage were totally independent of strain amplitude, the life should decrease linearly from A to C along the chain–dot line in Fig. 5. Instead, loading histories where the slow strain rate occurs near the maximum compressive strain (waveforms F, H, or K) produce little damage (i.e., they follow the horizontal line AD in Fig. 5, until the fraction of the strain history is sufficiently large that slow strain rates are occurring for strain amplitudes greater than the threshold. In contrast, for loading histories where the slow strain rate occurs near the maximum tensile strain (waveforms E, G, or H), life decreases continuously with the fraction of strain applied at the slow strain rate (line AB in Fig. 5), and then saturates as the fraction increases so that a portion of the slow strain rate now occurs at amplitudes less than the threshold value (line BC in Fig. 5). Thus, the hypothesis that each portion of the loading cycle above the threshold strain is equally damaging implies the decrease in fatigue life should follow line ABC when a slow rate occurs near the maximum tensile strain, and line ADC when it occurs near the maximum compressive strain.

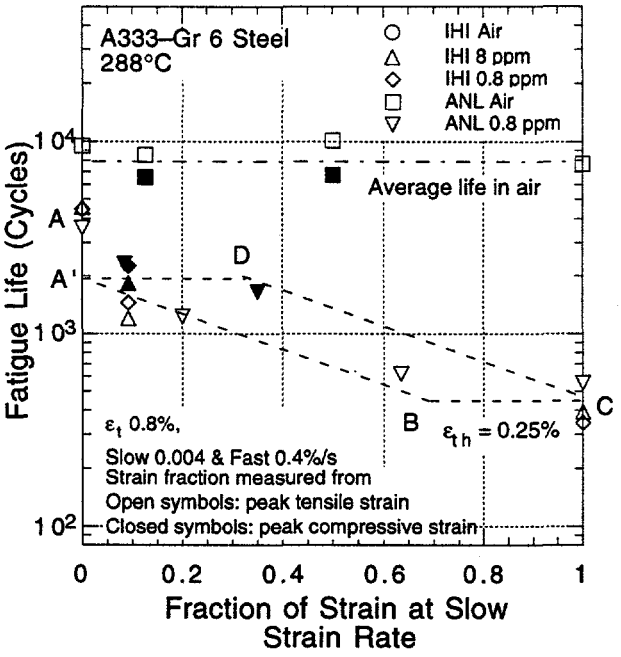

Figure 6.
Fatigue life of A333–Gr 6 carbon steel tested in air and water with loading waveforms where slow strain rate is applied during a fraction of the tensile cycle

Our conclusions appear to be in conflict with results from studies at IHI in Japan* that indicate that all portions of the tensile loading cycle are equally damaging, even the portion of the loading cycle that has only elastic strain. Fatigue tests were conducted on an IHI heat of A333–Gr 6 steel to try to resolve this issue.

The change in fatigue life of the IHI heat of A333–Gr 6 steel with fraction of loading strain at slow strain rate is shown in Fig. 6. Tests conducted at IHI in water containing 8 or 0.8 ppm DO are also included in the figure. The ANL and IHI test results are in good agreement. However, the data for this A333–Gr 6 steel appear to have a different trend than observed for the A106–Gr B steel used for the tests summarized in Fig. 5. For A333–Gr 6 steel, a slow strain rate near peak compressive strain appears to cause a significant reduction in fatigue life, whereas as discussed previously, steel slow strain rates only had a significant effect on fatigue of A106–Gr B when they occurred at strains greater than the threshold strain, which for this steel is ≈0.36%. We believe this apparent disagreement may be attributed to the effect of strain rate on fatigue life. A302–Gr B low–alloy steel and A333–Gr 6 carbon steel exhibit a strain rate effect in air, e.g., the fatigue life of both steels in air decreased ≈20% when the strain rate decreases from 0.4 to 0.004 %/s. In Fig. 6, we believe that the decrease in fatigue life from A to A' is most likely caused by a strain rate effect that is independent of the environment. Further decreases in strain rate are unlikely to have a significant effect on fatigue life in air. If the hypothesis that each portion of the loading cycle above the threshold strain is equally damaging is valid, the decrease in fatigue life due to environmental effects should follow line A'BC when a slow rate is applied near peak tensile strain and line A'DC when it is applied near peak compressive strain.

Progress Report on Experimental Research on Fatigue Life in LWR Environment, May 1993 to September 1994, prepared by Japanese EFD Committee, Thermal and Nuclear Power Engineering Society, presented at the Pressure Vessel Research Council meetings in New York, October 10–13, 1994.

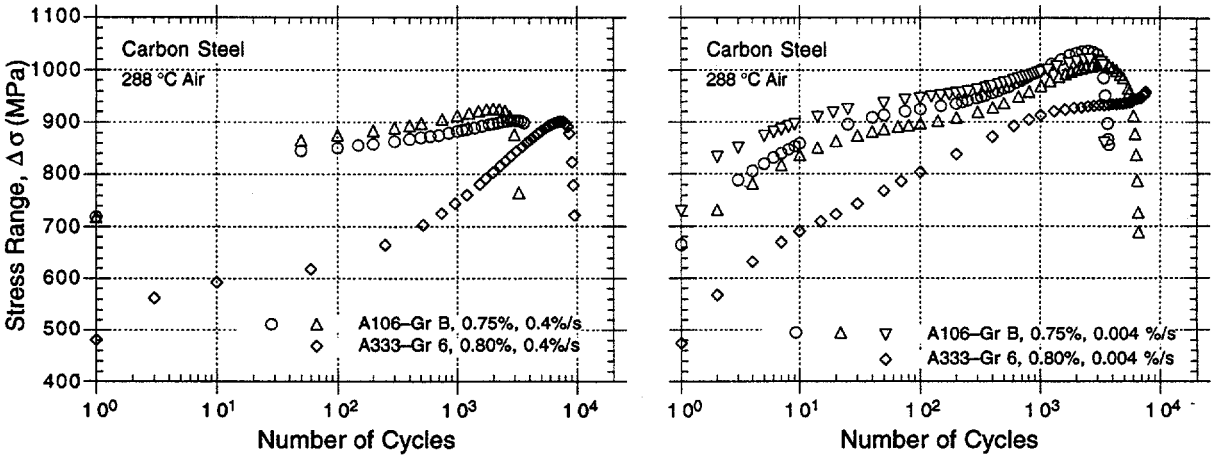

Figure 7. Effect of strain rate on cyclic strain–hardening behavior of A106–Gr B and A333–Gr 6 steels in air at 288°C and 0.75% strain range

Additional evidence of differences in behavior of the A106–Gr B and A333–Gr 6 steels is evident from the cyclic–hardening behavior. In Fig. 7, cyclic stress range is shown as function of the fatigue cycles for the two steels tested in air at 288°C, total strain range of 0.75 or 0.80%, and strain rates of 0.4 and 0.004 %/s. The A333–Gr 6 steel has a very low yield stress and shows significant cyclic hardening during the entire test. The A106–Gr B steel has a higher yield stress and exhibits a rapid cyclic hardening only during the initial 100 cycles. The latter also shows some dynamic strain aging at slow strain rates.

Environmentally Assisted Cracking of Alloy 600 and SSs in Simulated LWR Water

Besides its widespread use for steam generator tubing, Alloy 600 is used for a variety of structural elements in reactor systems. Cracking has been observed in a number of these components, e.g., instrument nozzles and heater thermal sleeves in the pressurizer,† penetrations for control–rod–drive mechanisms in reactor vessel closure heads in the primary system of PWRs,†† and in shroud–support–access–hole covers§ in BWRs. Experience strongly suggests that materials that are susceptible to SCC are also susceptible to environmental degradation of fatigue life and fatigue–crack–growth properties. Preliminary information on the effect of temperature, load ratio, and stress intensity on environmentally assisted cracking (EAC) of Alloys 600 and 690 in simulated BWR and PWR water has been obtained, and the crack growth rates (CGRs) of these materials have been compared with those of Type 316NG and sensitized Type 304 SS under conditions where EAC occurs in all materials.

The effect of water chemistry on CGRs of mill–annealed Alloy 600 and sensitized Type 304 SS was explored at a load ratio of 0.95 in water that contained ≈200 ppb DO. Small amounts of chromate and sulfate (<200 ppb) and two amines (1–5 ppm) produced small but measurable changes in the CGRs of the sensitized Type 304 SS specimens but had virtually no effect on the CGR of the Alloy 600 specimen. The CGR data for the three specimens are plotted in Fig. 8 versus the CGRs for wrought SSs in air predicted by the ASME Code Section XI correlation at the K_{max} and load ratio values used in the tests. The dashed and

†USNRC Information Notice No. 90–10, "Primary Water Stress Corrosion Cracking (PWSCC) of Inconel 600," Feb. 1990.

††INPO Document SER 20–93 "Intergranular Stress Corrosion Cracking of Control Rod Drive Mechanism Penetrations," Sept.1993.

§USNRC Information Notice No. 92–57, "Radial Cracking of Shroud Support Access Hole Cover Welds," Aug. 1992.

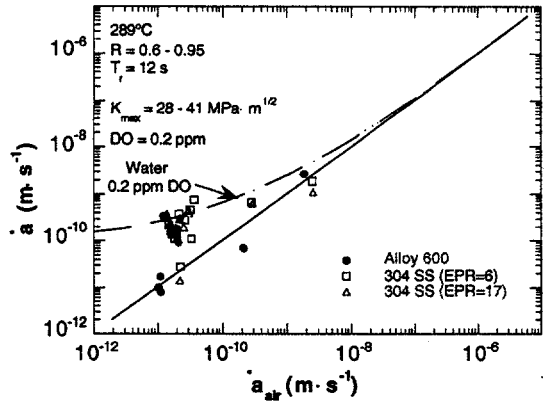

Figure 8.
Corrosion fatigue data for specimens of Alloy 600 and sensitized Type 304 SS in oxygenated water at 289°C. Dashed line represents ANL model predictions for austenitic SSs in water containing 0.2 ppm DO. Diagonal line corresponds to crack growth of SSs in air.

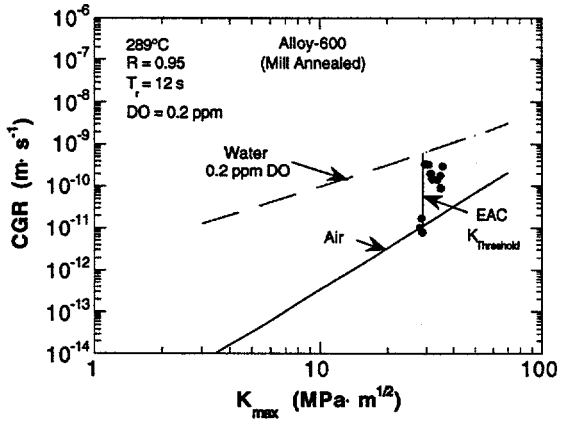

Figure 9.
Dependence of CGR of Alloy 600 specimen on K_{max} in oxygenated water at 289°C. Dashed and solid lines represent ANL model predictions for austenitic SSs in water containing 0.2 ppm DO and in air, respectively, at an R value of 0.95 and rise time of 12 s.

solid lines represent ANL model predictions for crack growth in water[11] and the "air line" predicted by the ASME Code, respectively. The data for all materials are bounded by the two curves. There appears to be a transition between the "air" curve and EAC behavior at a threshold corresponding to $\dot{a}_{air} \approx 2 \times 10^{11}$ m·s^{-1}. This threshold behavior can also be expressed in terms of K_{max} as shown in Fig. 9, which suggests a threshold K_{max} for EAC of ≈26 MPa·m$^{1/2}$ at an R of 0.95.

Corrosion–fatigue experiments were conducted on mill–annealed Alloy 600 and mill–annealed plus thermally treated Alloy 690 specimens to investigate the effects of temperature and dissolved oxygen and hydrogen in HP water on CGRs of these materials. The results are summarized in Fig. 10. At load ratios of 0.2 and 0.6, the CGRs are virtually independent of DO concentration or the ECP, which is not surprising, because at this load ratio, the CGRs are dominated by the mechanical cycling. At a higher load ratio of 0.9 where the environmental contribution is more significant, the CGRs decrease as the DO concentration or ECP decreases at 289 and 320°C. In all cases, the CGRs of both materials lie near or below the "air" curve for austenitic SSs. At an R ratio of 0.6, CGRs were typically higher in Alloy 690 than in Alloy 600. However, at an R ratio of 0.9, where the CGR dependence on DO concentration and ECP suggest that environmental enhancement is significant, CGRs in Alloy 600 were generally greater than those in the Alloy 690.

Experiments were also performed in simulated PWR primary–system water containing 450 ppm B and 2.25 ppm Li (added to the feedwater as H_3BO_3 and LiOH), 3–58 cm^3 H_2·kg^{-1} H_2O, and 750 ppb hydrazine,

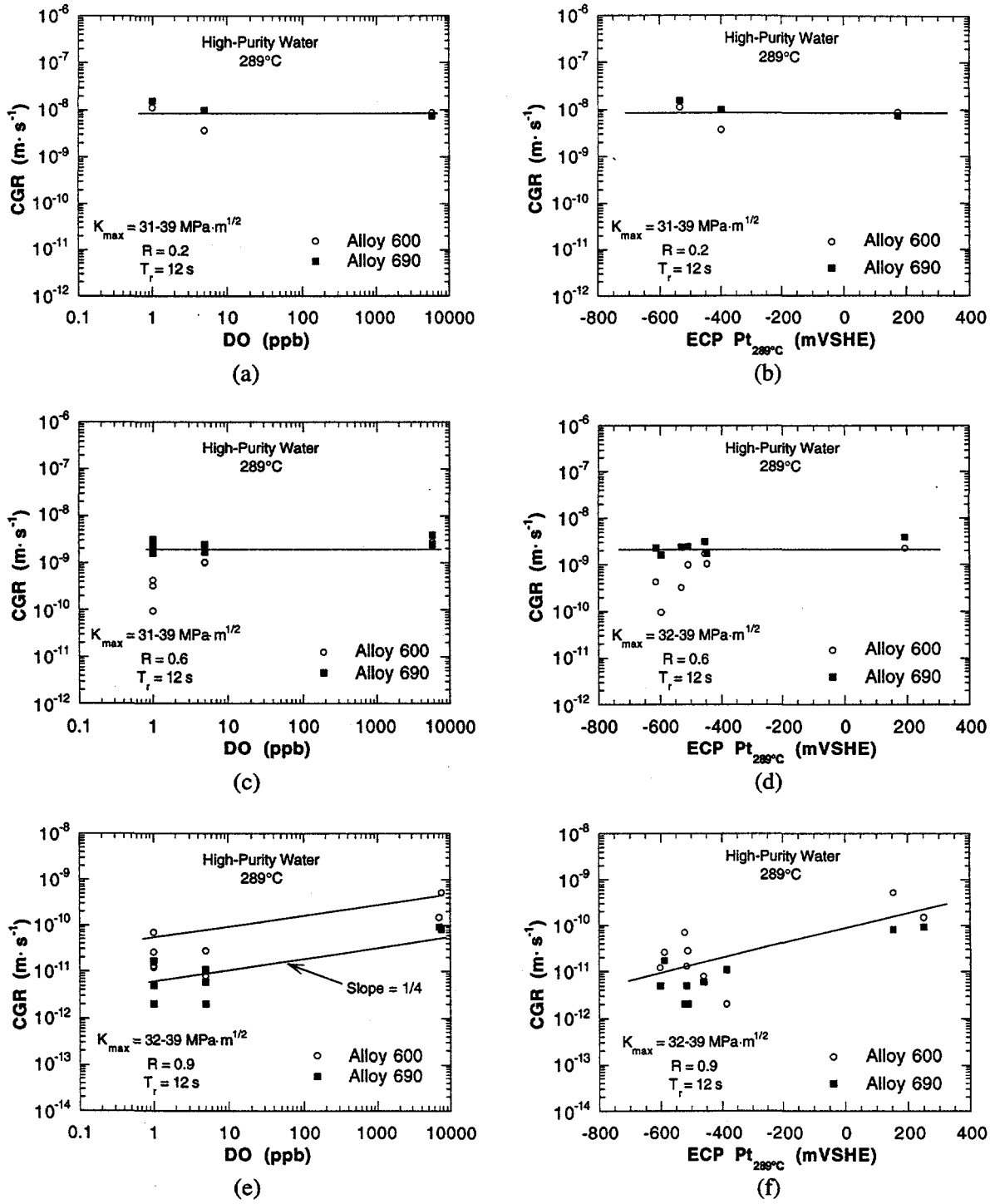

Figure 10. Dependence of CGRs of Alloy 600 and 690 specimens at 289°C on DO concentration in HP water and ECP of Pt electrode at 289°C at load ratios (R) of 0.2 (a and b), 0.6 (c and d), and 0.9 (e and f), respectively

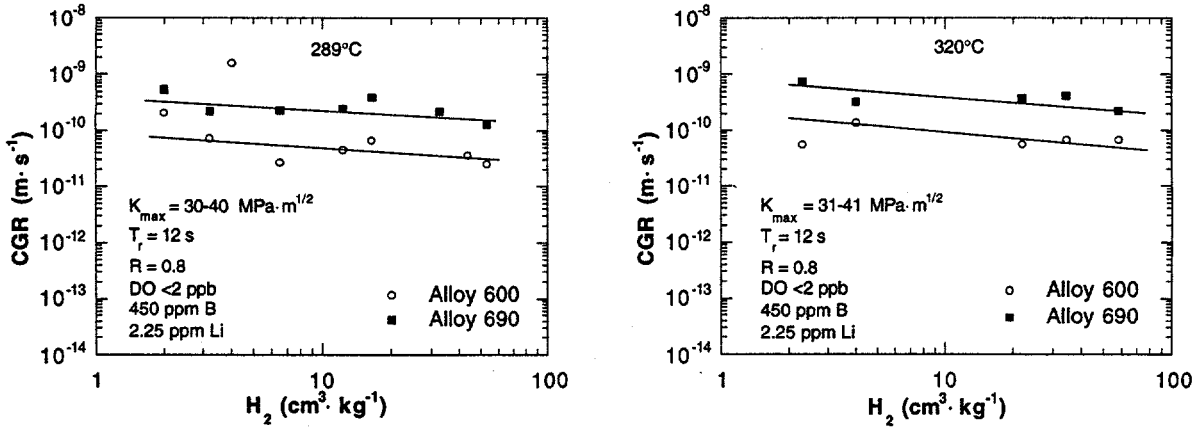

Figure 11. Dependence of CGRs of Alloy 600 and 690 specimens at (a) 289 and (b) 320°C on dissolved–H_2 concentration in simulated PWR water at load ratio of 0.8

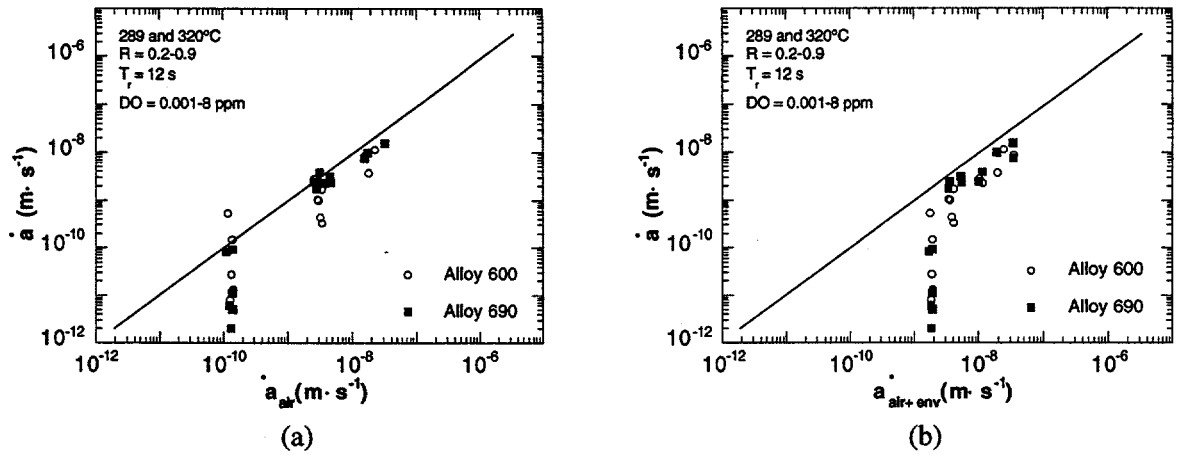

Figure 12. Corrosion fatigue data for Alloy 600 and 690 specimens in HP water at 289 and 320°C vs. (a) CGRs for SSs in air predicted by ASME Code, and (b) CGRs for SSs in water from ANL model, both under same loading conditions as in experiments. Lines represent identical CGRs for these alloys in test environments and for SSs (a) in air and (b) in water.

which was added to scavenge the residual DO to a very low level (≈1 ppb). The results of these tests are summarized in Fig. 11. At the load ratio R = 0.8 and water chemistry conditions used for these tests, the Alloy 690 specimen exhibited a higher CGR by a factor of ≈3 than Alloy 600 at both 289 and 320°C. Crack growth experiments will be conducted at higher load ratios, including constant load (R = 1.0), to determine whether Alloy 690 exhibits lower rates than Alloy 600 at higher R values. The CGRs decreased slightly as dissolved H_2 concentration increased from 3 to 58 $cm^3 \cdot kg^{-1}$. A somewhat larger decrease in the CGRs was expected based on a predicted change in the thermodynamic stability of NiO corrosion product on the alloys as the H_2 concentration of water increased, or as the temperature decreased in these experiments.

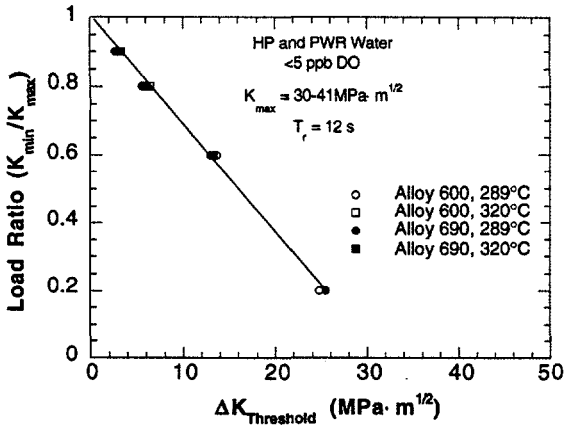

Figure 13.
Dependence of ΔK_{th} for Alloy 600 and 690 specimens in simulated PWR and de–oxygenated HP water on load ratio at 289 and 320°C

The CGRs for R ratios from 0.2–0.9 and DO concentrations from 0.001–8 ppm are plotted in Fig. 12 in terms of the CGR rate predicted by the ASME Section XI curve for SSs in air and the environmentally enhanced CGRs for SSs in water predicted by the correlations presented in Ref. 11. At very low CGRs the correlations are very conservative compared to the observed CGRs. The threshold values of ΔK as a function of load ratio R, corresponding to the threshold CGRs in Fig. 12, are shown in Fig. 13. Although only data at low DO are plotted in the figure, the results in Fig. 12 suggest that the results are valid even at higher DO levels. The dependence of $\Delta K_{Threshold}$ on load ratio can be expressed by a simple linear equation:

$$\Delta K_{th} = 32.0\,(1–R). \qquad (1)$$

SCC and Corrosion Fatigue of Austenitic and Aged Cast Stainless Steels

Most of the available data on corrosion fatigue of austenitic SSs in aqueous environments have been developed in support of LWR technology in the United States and abroad. Because Section XI of the ASME Code currently provides only an in–air design curve, corrosion fatigue data from the literature were analyzed to develop corrosion fatigue curves for SSs in aqueous environments. The results of this review were published in NUREG/CR–6176. At that time, there were few data available on CGRs in deaerated water at CGRs of 10^{-10} m·s^{-1} or less, which are of most interest in actual applications. Therefore, a conservative recommendation was made, i.e., correlations based on data obtained in water that contained ≈0.2 ppm DO should also be applied to low–oxygen environments characteristic of PWRs. Additional CGR tests on cast duplex and austenitic SSs have been performed to provide a technical basis for updating the correlations given in NUREG/CR–6176.

These tests indicated that CGRs in thermally aged cast SSs are similar to those in wrought SSs. In Fig. 14, measured CGRs for aged and nonaged cast SSs are compared with the predictions based on correlations for wrought SSs in NUREG/CR–6176. Tests in low–DO water show lower CGRs than in water with 0.2 ppm DO. Ford et al.[12] developed a detailed CGR model that includes the effects of DO (through changes in ECP). Based on SSRT tests, Kassner et al.[13] suggested that CGRs exhibit an $\approx[O_2]^{1/4}$ dependence on DO concentration. Predictions of both models are in reasonable agreement with the observed decreases in CGR corresponding to a decrease from 8 ppm to 200 ppb, but the model of Ford et al. predicts a significantly

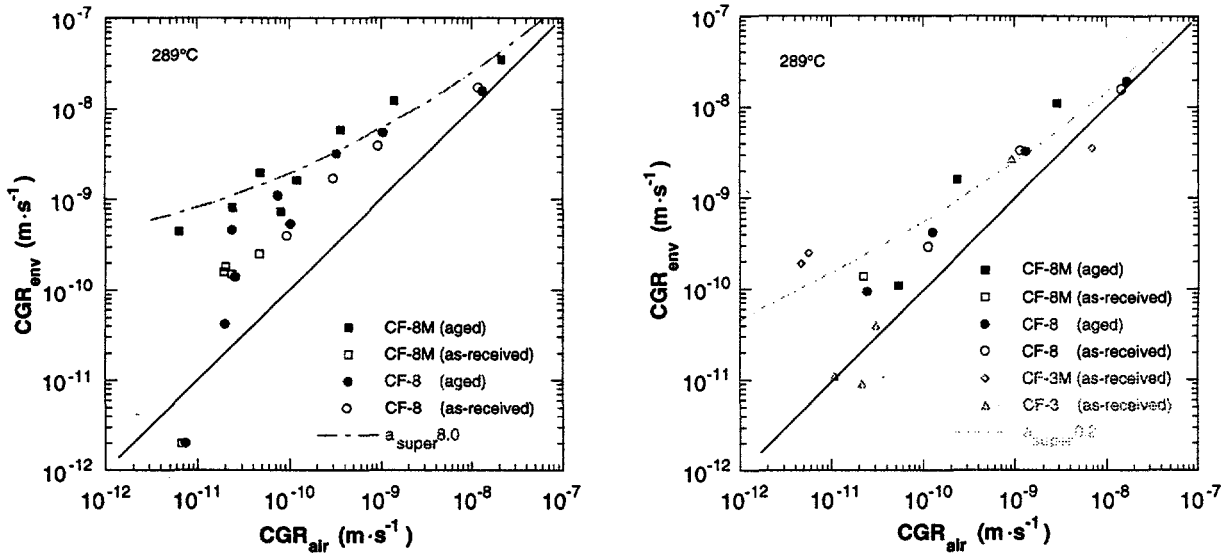

Figure 14. Corrosion fatigue data for as–received CF–3, –3M, and –8M and aged CF–8M and –8 cast SS in water containing 8 (left) and 0.2 (right) ppm DO at 289°C. Diagonal lines correspond to crack growth in air in Section XI of the ASME Code. Dashed lines indicate predictions from correlations in NUREG/CR–6176.

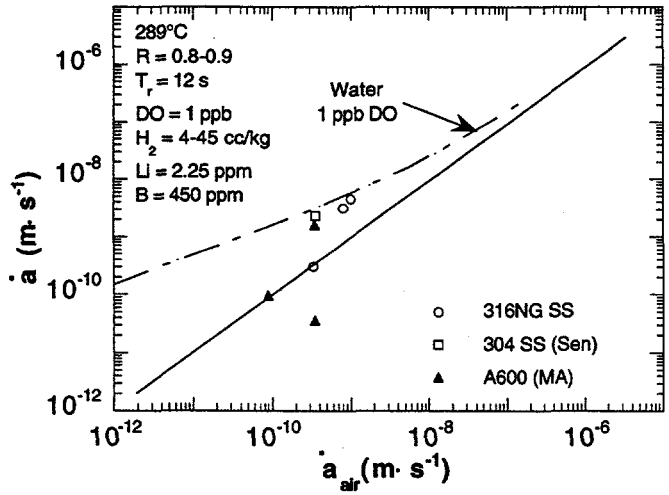

Figure 15.
Corrosion fatigue data for specimens of Alloy 600, Type 316NG and sensitized Type 304 SS in simulated PWR primary water at 289°C. Dashed line represents model predictions for austenitic SSs in water containing 1 ppb DO. Diagonal line corresponds to crack growth of SSs in air.

larger decrease in CGR than that of Kassner et al. when the DO decreases to ≈ 1 ppb. Revised correlations based on the latter model[13] are in good agreement with observed CGRs, as shown in Fig. 15.

Tests were also performed on Types 316NG and 304 SS and as–received and thermally aged CF–3 cast SS to investigate threshold stress intensity factors ΔK_{th}^{EAC} for EAC. Threshold behavior was clearly observed, as shown in Fig. 16, and the dependence of ΔK_{th}^{EAC} on load ratio for Types 347, 316NG, and sensitized 304 SS, and for thermally aged CF–3 and CF–8 grades of cast SS, was determined (Fig. 17). As in the case of Alloys 600 and 690, a simple linear relationship was observed:

$$\Delta K_{th}^{EAC} = 25.0(1 - R). \qquad (2)$$

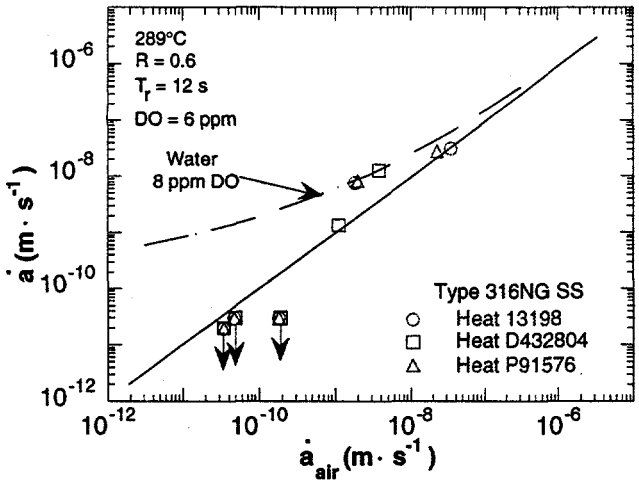

Figure 16.
Corrosion fatigue data for specimens from three heats of Type 316NG SS in HP oxygenated water at 289°C. Dashed line represents model predictions at an R value of 0.6 and rise time of 12 s in water containing 8 ppm DO. Solid line corresponds to crack growth of SSs in air.

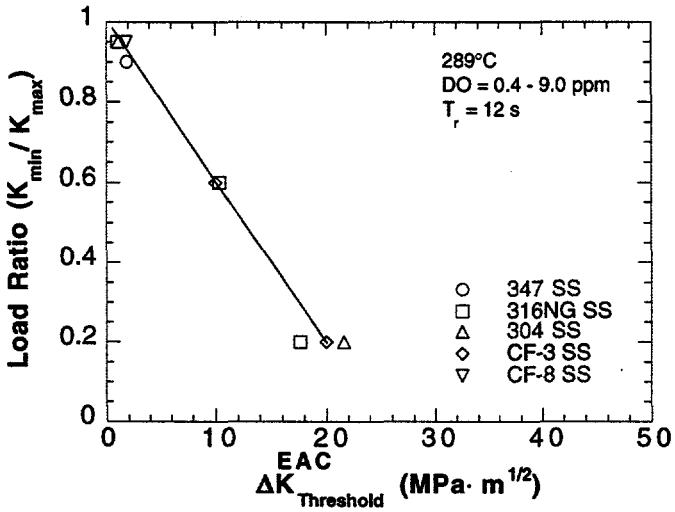

Figure 17.
Dependence of ΔK_{th} for EAC of wrought and cast austenitic SSs in HP oxygenated water at 289°C on load ratio

The correlations in NUREG/CR–6176 are being revised to include some "credit" for low DO in PWR environments. The data are being reviewed to determine whether thresholds can be included in the revised correlations.

References

1. M. Kodama, S. Nishimura, J. Morisawa, S. Shima, S. Suzuki, and M. Yamamoto, *Effects of Fluence and Dissolved Oxygen on IASCC in Austenitic Stainless Steels,* Proc. 5th Int. Symp. on Environmental Degradation of Materials in Nuclear Power Systems – Water Reactors, D. Cubicciotti, E. P. Simonen, and R. Gold, eds., American Nuclear Society, La Grange Park, IL, pp. 948-954 (1992).

2. M. Kodama, R. Katsura, J. Morisawa, S. Nishimura, S. Suzuki, K. Asano, K. Fukuya, and K. Nakata, *IASCC Susceptibility of Austenitic Stainless Steels Irradiated to High Neutron Fluence,* Proc. 6th Int.l Symp. on Environmental Degradation of Materials in Nuclear Power Systems - Water Reactors, R. E. Gold and E. P. Simonen, eds., The Minerals, Metals, and Materials Society, Warrendale, PA, pp. 583–588 (1993).

3. M. E. Indig, J. L. Nelson, and G. P. Wozadlo, *Investigation of the Protection Potential Against IASCC,* Proc. 5th Int. Symp. on Environmental Degradation of Materials in Nuclear Power Systems – Water Reactors, D. Cubicciotti, E. P. Simonen, and R. Gold, eds., American Nuclear Society, La Grange Park, IL, pp. 941–947 (1992).

4. H. M. Chung, W. E. Ruther, and J. E. Sanecki, in *Environmentally Assisted Cracking in Light Water Reactors: Semiannual Report, October 1993–March 1994,* NUREG/CR–4667 Vol. 18, ANL–95/2, pp. 27–35 (March 1995).

5. C. T. Ward, D. L. Mathis, and R. W. Staehle, *Intergranular Attack of Sensitized Austenitic Stainless Steel by Water Containing Fluoride Ions,* Corrosion **25,** 394–396 (1969).

6. N. C. Huang and Z. Nagy, *Kinetics of the Ferrous/Ferric Electrode Reaction in the Absence of Chloride Catalysis,* J. Electrochem. Soc. **134**, 2215–2220 (1987).

7. S. Kasahara, K. Nakata, K. Fukuya, S. Shima, A. J. Jacobs, G. P. Wozadlo, and S. Suzuki, *The Effects of Minor Elements on IASCC Susceptibility in Austenitic Stainless Steels Irradiated with Neutrons,* in Proc. 6th Int. Symp. on Environmental Degradation of Materials in Nuclear Power Systems - Water Reactors, R. E. Gold and E. P. Simonen, eds., The Minerals, Metals, and Materials Society, Warrendale, PA, pp. 615–622 (1993).

8. O. K. Chopra, W. F. Michaud, and W. J. Shack, in *Environmentally Assisted Cracking in Light Water Reactors, Semiannual Report, April–September 1994,* NUREG/CR–4667 Vol. 19, ANL–95/25, pp. 3–18 (Sept. 1995).

9. O. K. Chopra and W. J. Shack, *Effects of LWR Environments on Fatigue Life of Carbon and Low–Alloy Steels*, in Fatigue and Crack Growth: Environmental Effects, Modeling Studies, and Design Considerations, PVP Vol. 306, S. Yukawa, ed., American Society of Mechanical Engineers, New York, pp. 95–109 (1995).

10. O. K. Chopra and W. J. Shack, *Effects of Material and Loading Variables on Fatigue Life of Carbon and Low–Alloy Steels in LWR Environments*, in Transactions of the 13th Int. Conf. on Structural Mechanics in Reactor Technology (SMiRT 13), Vol. II, M. M. Rocha and J. D. Riera, eds., Escola de Engenharia – Universidade Federal do Rio Grande do Sul, Porto Alegre, Brazil, pp. 551–562 (1995).

11. W. J. Shack and T. F. Kassner, *Review of Environmental Effects on Fatigue Crack Growth of Austenitic Stainless Steels*, NUREG/CR–6176, ANL–94/1, (May 1994).

12. F. P. Ford, D. F. Taylor, P. L. Andresen, and R. Ballinger, *Corrosion-Assisted Cracking of Stainless and Low-alloy Steels*, EPRI NP-5064s, Electric Power Research Institute, Palo Alto, CA (February 1987).

13. T. F. Kassner, W. E. Ruther, and W. K. Soppet, *Mitigation of Stress Corrosion Cracking of AISI 304 Stainless Steel by Organic Species at Low Concentrations in Oxygenated Water,* Corrosion 90, Paper No. 489, Las Vegas, NV (April 1990).